Application of recurrence quantification analysis of acoustic emission time series to analysis of a plastic flow of metals

Einar A. Agletdinov* and Igor S. Yasnikov
Research Institute for Advanced Technologies, Togliatti State University, Togliatti 445020, Russia

(Received 9 June 2023; accepted 2 October 2023; published 26 October 2023)

As a result of the application of recurrence quantification analysis to acoustic emission time series obtained in uniaxial tensile testing of copper and silver, we detected the existence of a characteristic interval in which the Shannon information entropy (as a parameter of the quantitative analysis of recurrence plots) increased rapidly. Using statistical analysis of the behavior of the dislocation ensemble, we established a relation between the physical parameters of the given interval and the global stability loss parameters of the plastic flow of metals, indicating the predictability of the distinctive point determined long before the critical state was attained.

DOI: 10.1103/PhysRevE.108.044217

I. INTRODUCTION

The recurrence plot method proposed by Eckmann *et al.* [1] is a popular tool for nonlinear time series analysis along with Lyapunov exponents [2], multifractal analysis [3], and analysis of correlation dimension [4]. The rapid development of the recurrence plot method during the last two decades has led to the emergence of *recurrence quantification analysis* (RQA) that has found its application in a wide range of fields, including seismology [5], astrophysics [6,7], economics [8], and biological science [9,10]. RQA is based on the reconstruction of the phase portrait of a dynamical system from a single observed time series and makes it possible to characterize the behavior of nonlinear systems not only qualitatively but also quantitatively; it permits the identification of transitions between different stages of processes and phenomena being investigated.

In this sense, the acoustic emission (AE) induced by the deformation of solids [11,12] can precisely reflect the dynamics of defects ensemble and, representing a time series, can be a good indicator in testing RQA methods. Despite this, the cases of RQA application to AE time series in metals are rare; for example, this method has been employed in Ref. [13] for studying the corrosion of magnesium alloys. Most of the publications in this field are devoted to the investigation of rocks in the context of geophysical studies [14,15].

The RQA method is based on the assumption of the existence of a specific dynamical system represented as d autonomous differential equations:

$$\frac{d\mathbf{x}}{dt} = \mathbf{F}(\mathbf{x}), \tag{1}$$

where $\mathbf{x}(t) = x_1(t), x_2(t), \ldots, x_d(t)$ is a vector in the phase space of dimension d, which unambiguously and comprehensively characterizes the state of the system at time t in given initial conditions. However, the system of equations for a dynamical system can be written only in some rare cases. The most effective and classically successful example is the system of Lorentz equations [16]. However, in practice, there often exist some observable physical quantities represented in the form of time series. The AE signals detected during plastic deformation of metals reflect the dynamics of numerous nonlinearly interacting spatially distributed local stress relaxation events which, being spatially and temporarily integrated, cause the macroscopically homogeneous deformation of the entire material. Given the strong nonlinearity of the system, a single variable can contain substantial information on the behavior of the system as a whole. The latter fact stimulated the development of the entire class of nonlinear dynamics methods based on the phase space reconstruction from a single observable [17].

Let us consider in detail the quantitative analysis of recurrence plots. Let $u_i = u_1, u_2, \ldots, u_N$ be an observed time series of length N. Then the reconstruction of the state vector based on the Takens theorem [18] will be given by $\hat{\mathbf{x}}_i = [u_i, u_{i+\tau}, u_{i+2\tau}, \ldots, u_{i+(m-1)\tau}]$. Here, the following parameters of the phase space trajectory reconstruction are introduced: τ is the time delay, and m is the embedding dimension. To avoid distortions that may lead to erroneous interpretations and conclusions, it is important to determine the optimal values of parameters τ and m. According to Ref. [19], the optimal value of τ is chosen as the value for which mutual information attains the first minimum. Then the optimal embedding dimension m is determined by the Cao method [20].

A recurrence plot shows the times for which the reconstructed phase trajectory returns to the small neighborhood of a certain point and is a graphic representation of the recurrence matrix defined as

$$R_{ij} = \theta(\delta - \|\hat{x}_i - \hat{x}_j\|), \quad i, j = 1, 2, \ldots, M, \quad \text{where} \quad M = N - \tau(m-1). \tag{2}$$

Here, δ is the radius of the small neighborhood, indices i and j count the discrete time, $\|\hat{\mathbf{x}}_i - \hat{\mathbf{x}}_j\|$ is the distance between

*aeinar7@gmail.com

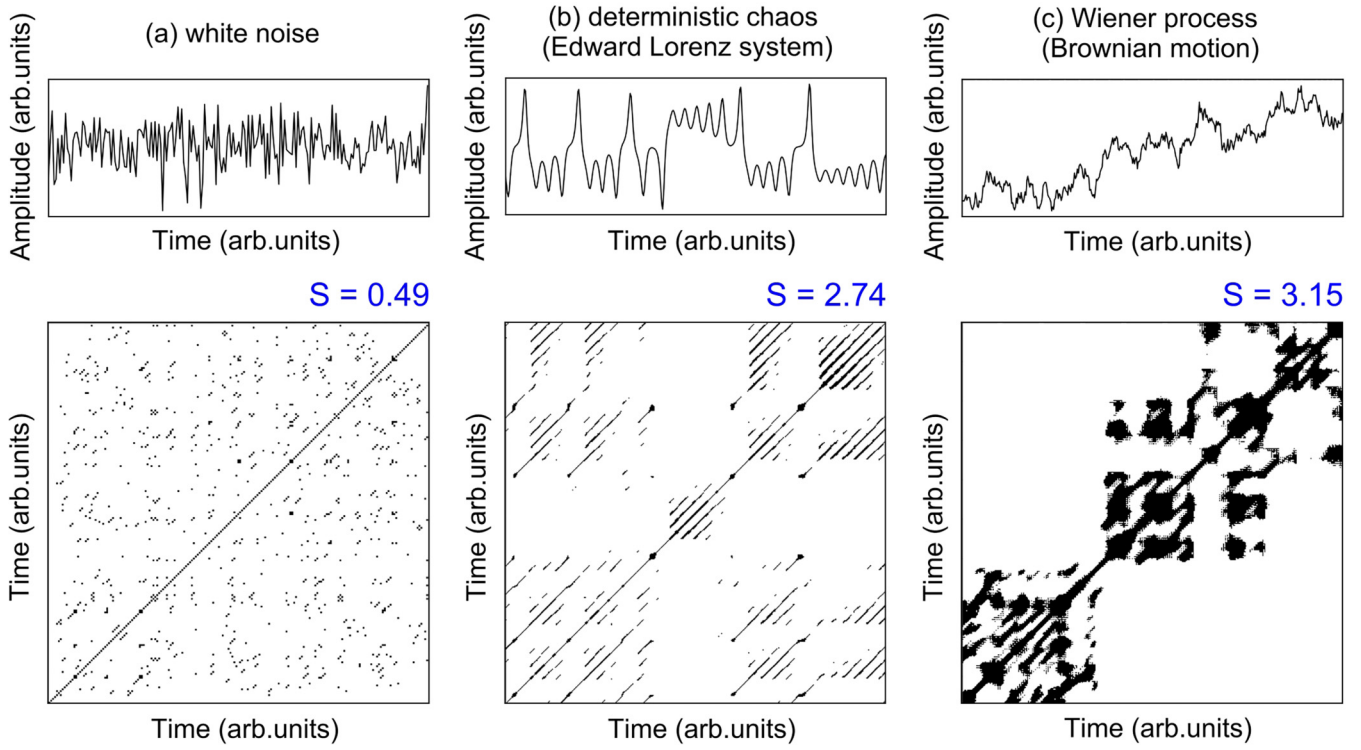

FIG. 1. Examples of recurrence plots for different artificially generated time series.

the phase trajectories at the instants of time i and j, and $\theta(u)$ is the Heaviside function. The recurrence matrix R_{ij} consists of zeros and unities which correspond to white and black pixels forming the vertical and diagonal lines, separate points, and other structures on the recurrence plot. Figure 1 shows examples of recurrence plots for artificially generated time series. Individual points are produced by strongly fluctuating trajectories, which is typical of noise signals [white noise, Fig. 1(a)]. Diagonals appear on the recurrent diagram when a segment of the phase trajectory runs parallel to an adjacent segment, which is typical of quasiperiodic segments of the time series. For this reason, systems with an exponential sensitivity to the initial conditions are characterized by short diagonals with an irregularly varying length [deterministic chaos determined by the system of Lorentz equations, Fig. 1(b)]. Random processes are characterized by dense irregular structures and empty white zones due to nonstationarity [Wiener process or Brownian motion, Fig. 1(c)].

Although the visual analysis of recurrence plots makes it possible to identify qualitatively various regimes and transitions between them [21,22], it is more effective to use parameters characterizing small-scale structures on recurrence plots quantitatively, which is the essence of RQA. Using a small-length window sliding over a time series, it is possible to determine the behavior of these parameters depending on time. Some investigations show that RQA parameters can reveal bifurcation points, including the chaos-order and chaos-chaos transitions [21,23]. In pioneering work on RQA [22], five basic parameters were proposed: *Recurrent density* (percentage of recurrent points on the recurrent diagram), *determinism* (percentage of points forming only diagonal lines), the *ratio of determinism to recurrent density, trend* (the quantity characterizing the displacement of points from the principal diagonal), and *Shannon entropy* of the frequency distribution of diagonal line lengths. The latter quantity is defined as

$$S = -\sum_{l=l_{\min}}^{M} p(l)\ln[p(l)], \tag{3}$$

where $l_{\min}$ is the minimal length of the diagonal l, and $p(l)$ is the probability that the length of the diagonal equals to l, which is defined by the following expression:

$$p(l) = H(l) \Big/ \sum_{l \geqslant l_{\min}}^{M} H(l), \tag{4}$$

where $H(l)$ is the histogram of the lengths of diagonal lines:

$$H(l) = \sum_{i,j=1}^{M} (1 - R_{i-1,j-1})(1 - R_{i+1,j+1}) \prod_{k=0}^{l-1} R_{i+k,j+k}. \tag{5}$$

Information entropy S reflects the amount of information required for describing the complex structure of the recurrence plot, namely, its diagonal components. Therefore, it can be interpreted as a measure of complexity of the underlying dynamics. For example, to describe the recurrence plot consisting only of diagonals of the same length, only one number, diagonal length (i.e., a small amount of information), is required. Accordingly, white noise is also characterized by low-information entropy [Fig. 1(a), $S = 0.49$]. For describing a recurrence plot consisting of many diagonals of different lengths, one must know the length distribution, i.e., a large amount of information is required. Therefore, it is assumed

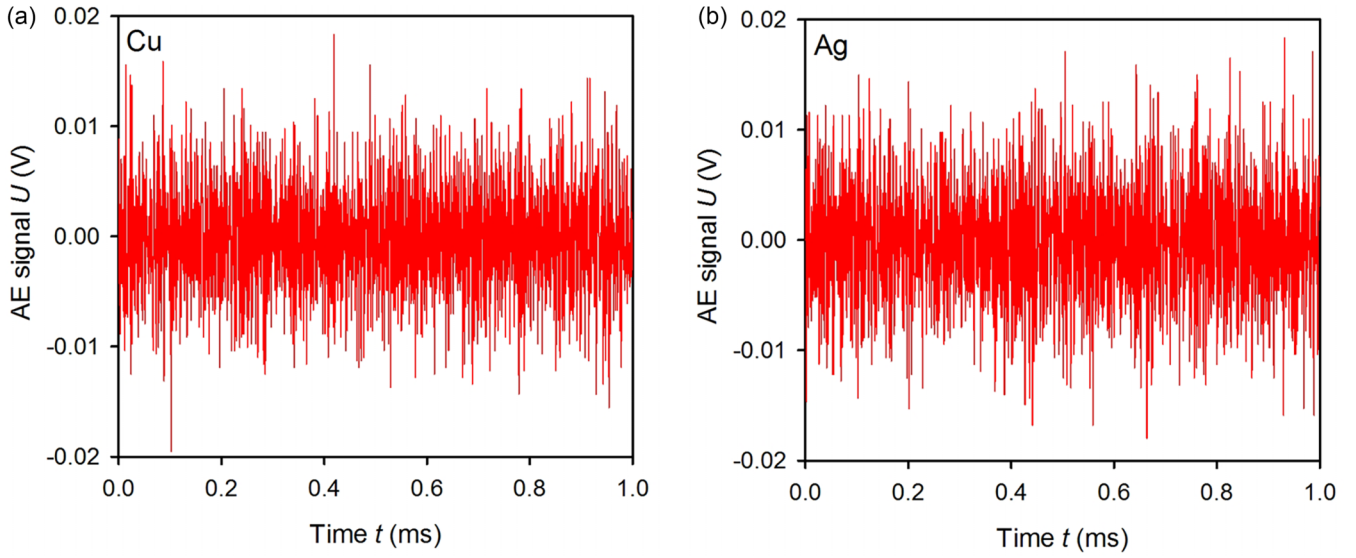

FIG. 2. Fragments of continuous random acoustic emission signals obtained under uniaxial plastic deformation of (a) copper and (b) silver.

that information entropy reflects the degree of complexity of the recurrence plot. Deterministic chaos is characterized by recurrence plots with many diagonals of various lengths and hence by high-information entropy [Fig. 1(b), $S = 2.74$]. Stochastic processes generating dense structures of irregular shapes are characterized by still higher values of entropy [Fig. 1(c), $S = 3.15$].

In this paper, we apply RQA to reveal and interpret specific features of AE time series, which were registered under plastic deformation of representative face-centered cubic (fcc) metals. Since the AE method is a universal tool for describing the evolution of the dislocation structure of a material under loading, the predictability of this tool as regards the emergence of peculiarities of a plastic flow and the emergence of the critical state is quite promising for laboratory experiments as well as for practical application in monitoring and diagnostic systems in the industry [12].

II. EXPERIMENTAL TECHNIQUE

As the material for investigation, we chose polycrystals of pure (99.99%) fcc metals (copper and silver). Using spark erosion cutting, we prepared two-dimensional (2D) samples of size 15 × 7 × 2 mm for uniaxial tensile tests. As a result of vacuum annealing for 90 min at a temperature of 0.85 of the melting temperature, we obtained a grain size of 100 ± 35 μm for copper and 90 ± 70 μm for silver. Uniaxial tensile tests were performed on a Tinius Olsen H50KT universal test machine with a 5 kN strain-gauge load cell and a precision system for strain measurements using an extensometer with a resolution of 1 μm, which ensured a constant strain rate of 2×10^{-3} s^{-1}.

Mechanical tests were accompanied by continuous registration of an AE signal by an NF AE-900S WB broadband piezoelectric transducer in the frequency range of 100–900 kHz. The transducer was connected to a low-noise PAC 2/4/6 amplifier with an amplification factor of +60 dB, and the AE signal was recorded using a PAC (Physical Acoustic Corporation, USA) PCI-2board with a sampling rate of 2 MHz.

Despite the discreteness of the dislocation slip lines, the AE signal detected under loading of fcc metals integrates the contribution from many slip events, which can coincide or occur sequentially with short interevent intervals. AE is, therefore, a continuous random process [11]. Figure 2 shows examples of the fragments of continuous AE signals obtained under uniaxial plastic deformation of copper [Fig. 2(a)] and silver [Fig. 2(b)]. The detection of individual events in continuous AE streams emerging during plastic straining of pure metals is challenging (or even impossible), and threshold-less registration of a continuous signal with a high sample rate is used. For further analysis, the AE parameters, such as power and energy calculated by a sliding window, are conventionally used [24–26]. In this paper, we used the amplitude calculated by a sliding window of length 260 ms with a step of 26 ms as the integral characteristic of the AE time series. The sample rate of the resulting amplitude time series was 38 Hz. Figure 3 shows the time dependences of the true stress and the AE signal amplitude calculated by the sliding window with the given parameters, which have been obtained for uniaxial loading of copper [Fig. 3(a)] and silver [Fig. 3(b)].

The resulting time series of the AE amplitude shown in Fig. 3 were subjected to RQA. The optimal embedding parameters were determined by the procedures mentioned above [19,20] and were $m = 9$, $\tau = 2$, and $\delta = 9 \times 10^{-3}$ for copper and $m = 9$, $\tau = 2$, and $\delta = 8.5 \times 10^{-3}$ for silver. Shannon information entropy S was calculated using the expressions in Eqs. (3)–(5) by a sliding window of lengths 40 and 43 s with steps of 13 and 10 s for silver and copper, respectively. The resulting time dependences of the information entropy are shown in Figs. 4(a) and 4(b) for copper and silver, respectively. It should be noted that the obtained $S(t)$ dependences display an entropy jump followed by an increase of both curves. The characteristic time interval corresponding to the abrupt change in the entropy was chosen as the first segment that violated the initial trend of the information entropy constancy (in Fig. 4, it is shown in gray).

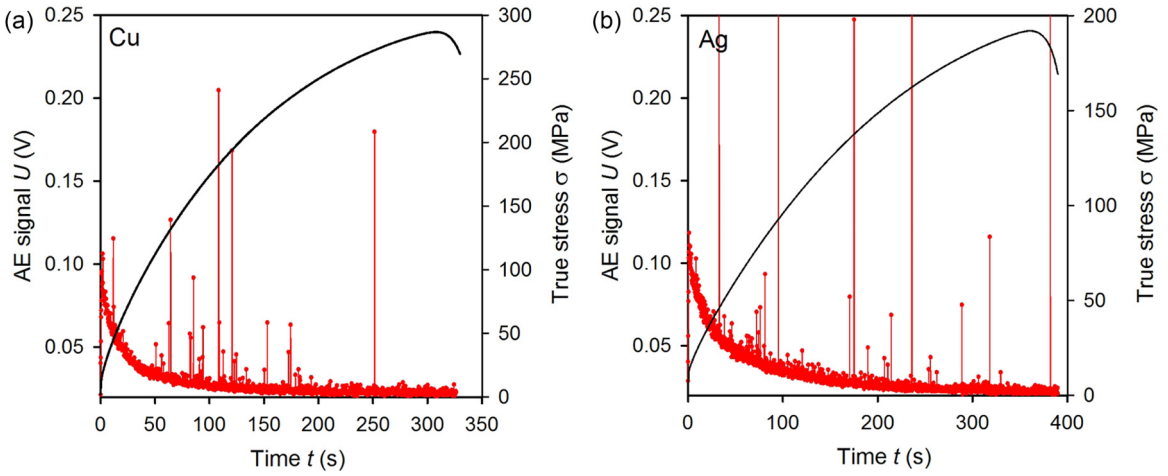

FIG. 3. Time dependences of the true stress and acoustic emission (AE) signal amplitude calculated by a sliding window and obtained under uniaxial straining of (a) copper and (b) silver.

III. THEORETICAL SUBSTANTIATION OF RESULTS AND DISCUSSION

The state of the deformed metal, in which a sharp change in the general trend of information entropy variation has been detected does not correspond to the point of macroscopic plastic flow stability loss (Considère point [27]). Rather, it is observed at the stable stage of strain hardening, as will be demonstrated in what follows. The emergence of the point at which the general information entropy trend changes is associated with the features of dislocation ensemble evolution. Therefore, to identify the physical origin of the given point, we used the simplest and most commonly adopted Kocks-Mecking (KM) phenomenology [28] with the evolution equation of the form:

$$\frac{d\rho}{d\gamma} = k_1\sqrt{\rho} - k_2\rho, \tag{6}$$

where ρ is the dislocation density, γ is the shear strain, and k_1 and k_2 are phenomenological coefficients. The first term on the right-hand side of Eq. (6) describes the multiplication of dislocations due to the dislocation forest, while the second term describes their annihilation during dislocation recovery. This phenomenological approach has been successfully employed in the analysis of the evolution of dislocation density on many occasions (notably on the examples of samples tested in this paper).

It is worth noticing here that the phenomenological equations of the KM model can be derived from the basics of nonequilibrium dislocation ensemble thermodynamics [29]. The obtained values of the coefficients describing the production, multiplication, and annihilation of dislocations include only physically measurable properties of the material and do not contain explicit uncertainties. The KM formulation of the dislocation kinetics represents a simplistic single internal variable integral approach which has pros and cons. Apparently, it misses many details of the dislocation behavior such as slip multiplication on each system due to cross-slip of screw dislocations or dislocation loop generation at glissile junctions [30,31]. There have been many modifications

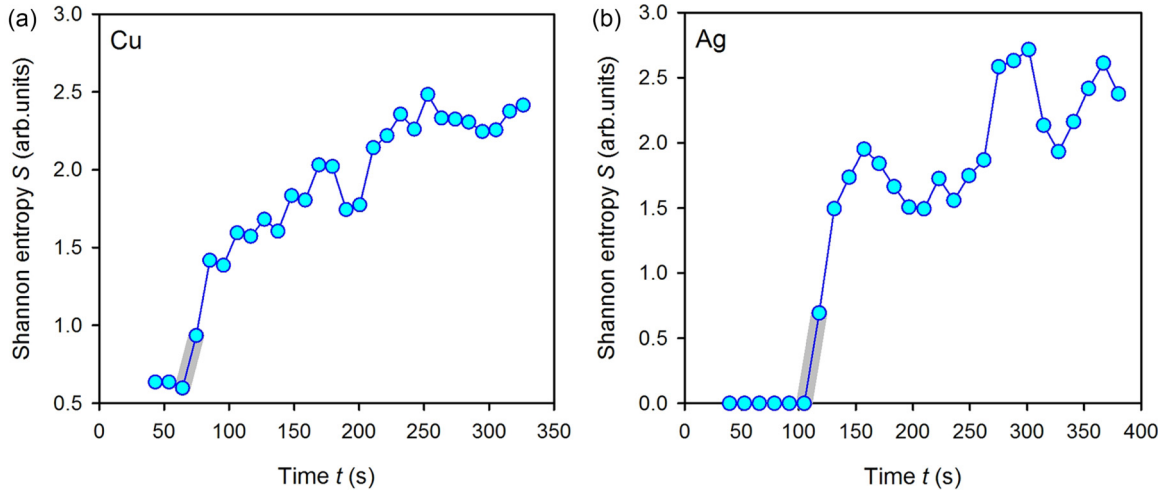

FIG. 4. Time dependences of information entropy for (a) copper and (b) silver. The characteristic interval of the jump-wise change in the information entropy, in which the initial trend of its constancy has been violated for the first time, is shown in gray.

proposed to enhance the KM model, attempting to capture various microstructural factors by introducing additional terms or employing two or more internal variables [28,32,33]. The versatility of modified models permits precise approximation of a wide range of experimental stress-strain data. Although detailing various dislocation reactions is possible in this way, it occurs at a price—the analytical transparency is lost. Aiming at keeping as small a number of parameters as possible and avoiding redundant complexity without compromising the accuracy of the strain hardening prediction, the first-order approximation KM approach is most appealing. We shall demonstrate in what follows that, although the simplest form of the KM model is employed, it reproduces the experimental stress-strain curves quite well. As a bonus, the simplicity and conciseness of the model ensures straightforward application of the fluctuation analysis and clear interpretation of the results.

In what follows, we will use the approach proposed in Ref. [34], assuming the dislocation density and the shear-strain rate are considered fluctuating physical quantities. To implement this approach, we rewrite Eq. (6) as

$$\frac{d\rho}{dt} = \dot{\gamma}(k_1\sqrt{\rho} - k_2\rho). \tag{7}$$

The fact that the dislocation ensemble density fluctuates has been discussed in detail in Ref. [11]. Let us suppose that, on a certain segment of the loading curve corresponding to strain rate $\dot{\gamma}$ and dislocation density ρ, their fluctuations are $\delta\dot{\gamma}$ and $\delta\rho$, respectively. Then in accordance with Eq. (7), these fluctuations satisfy the following condition:

$$\frac{d(\rho+\delta\rho)}{dt} = (\dot{\gamma}+\delta\dot{\gamma})[k_1\sqrt{\rho+\delta\rho} - k_2(\rho+\delta\rho)]. \tag{8}$$

Opening the brackets in this equation, disregarding the second-order terms (product of fluctuations), and subtracting Eq. (7) from the resulting expression, we obtain

$$\delta\dot{\rho} = k_1\left(\frac{\dot{\gamma}\delta\rho}{2\sqrt{\rho}} + \sqrt{\rho}\delta\dot{\gamma}\right) - k_2(\dot{\gamma}\delta\rho + \rho\delta\dot{\gamma}). \tag{9}$$

In this expression, the phenomenological constant k_1 can be eliminated using Eq. (6) in the form $k_1 = (\frac{d\rho}{d\gamma} + k_2\rho)/\sqrt{\rho}$, which immediately yields

$$\delta\dot{\rho} = \frac{1}{2\rho}\left(\frac{d\rho}{d\gamma} - k_2\rho\right)\dot{\gamma}\delta\rho + \frac{d\rho}{d\gamma}\delta\dot{\gamma}.. \tag{10}$$

In addition, we will use the Taylor relation connecting the true flow stress and the dislocation density:

$$\sigma = \alpha GMb\sqrt{\rho} = \beta\sqrt{\rho}, \tag{11}$$

where $\alpha \sim 0.4$–0.5, G is the shear modulus, b is the magnitude of Burger's vector of the dislocation, and M is the orientation factor. At variance with our previous work [34], we dropped the strain rate sensitivity in Eq. (11) for clarity, bearing in mind that the strain rate sensitivity is fairly small for fcc metals. The use of this equation with explicit strain rate sensitivity has led to cumbersome mathematical expressions. This resulted in the incomplete stability analysis in Ref. [34], where the only global loss of plastic flow stability was considered, whereas the second characteristic point was not considered. Without contradictions with the previous work, this issue is addressed in this paper.

With an account for the sample incompressibility condition $\delta\sigma = \sigma\delta\varepsilon$ [34] (ε is the true axial strain, $\varepsilon = \gamma/M$) and the variation of the Taylor relation in Eq. (10), we can quickly obtain the following chain of equalities:

$$\delta\gamma = M\delta\varepsilon = M\frac{\delta\sigma}{\sigma} = M\frac{\beta\frac{\delta\rho}{2\sqrt{\rho}}}{\beta\sqrt{\rho}} = M\frac{\delta\rho}{2\rho}. \tag{12}$$

Assuming the time dependence of fluctuations in the form:

$$\begin{cases} \delta\rho = x = x_0\exp(\lambda t) \\ \delta\gamma = y = y_0\exp(\lambda t) \end{cases} \quad \begin{cases} \delta\dot{\rho} = \dot{x} = x_0\lambda\exp(\lambda t) \\ \delta\dot{\gamma} = \dot{y} = y_0\lambda\exp(\lambda t) \end{cases}, \tag{13}$$

and substituting these expressions into Eqs. (10) and (12), we obtain the following linear system of equations:

$$\left[\lambda - \frac{\dot{\gamma}}{2\rho}\left(\frac{d\rho}{d\gamma} - k_2\rho\right)\right]x_0 = \left[\frac{d\rho}{d\gamma}\lambda\right]y_0$$
$$\left[\frac{M}{2\rho}\right]x_0 = y_0. \tag{15}$$

The compatibility of this linear system leads to the characteristic equation:

$$\lambda\left(1 - \frac{M}{2}\frac{1}{\rho}\frac{d\rho}{d\gamma}\right) = \frac{\dot{\gamma}}{2}\left(\frac{1}{\rho}\frac{d\rho}{d\gamma} - k_2\right). \tag{16}$$

With an account for the Taylor relation in Eq. (11), Eq. (16) is transformed to

$$\lambda\left(1 - \frac{1}{\sigma}\frac{d\sigma}{d\varepsilon}\right) = \frac{\dot{\gamma}}{2}\left(\frac{2}{M}\frac{1}{\sigma}\frac{d\sigma}{d\varepsilon} - k_2\right). \tag{17}$$

Assuming exponential relaxation of the amplitude of dislocation density fluctuations in Eq. (13), the decay of the fluctuation amplitude requires the negativity of the exponent, which immediately leads to the condition $\lambda < 0$.

This immediately leads to a system of inequalities which must be fulfilled for the plastic flow to be stable:

$$\frac{1}{\sigma}\frac{d\sigma}{d\varepsilon} > \frac{k_2M}{2}$$
$$\frac{1}{\sigma}\frac{d\sigma}{d\varepsilon} > 1. \tag{18}$$

For convenience, let us introduce unified variables [35]:

$$\sigma_S = \frac{\beta k_1}{k_2}, \quad \frac{1}{\tilde{\varepsilon}} = \frac{k_2M}{2}, \quad \frac{\sigma_S}{\tilde{\varepsilon}} = \frac{k_1M\beta}{2}. \tag{19}$$

Then combining the KM evolution in Eq. (6) with Eq. (11), one obtains the equation for the flow stress in the form:

$$\frac{d\sigma}{d\varepsilon} = \frac{1}{\tilde{\varepsilon}}(\sigma_S - \sigma). \tag{20}$$

Solving this equation with the initial condition $\sigma(\varepsilon = 0) = \sigma_0$ (σ_0 is the initial strain hardening connected with initial dislocation density ρ_0 by the relation $\sigma_0 = \beta\sqrt{\rho_0}$) yields the explicit form of the stress-strain relationship as

$$\sigma(\varepsilon) = \sigma_0 + (\sigma_S - \sigma_0)\left[1 - \exp\left(-\frac{\varepsilon}{\tilde{\varepsilon}}\right)\right]. \tag{21}$$

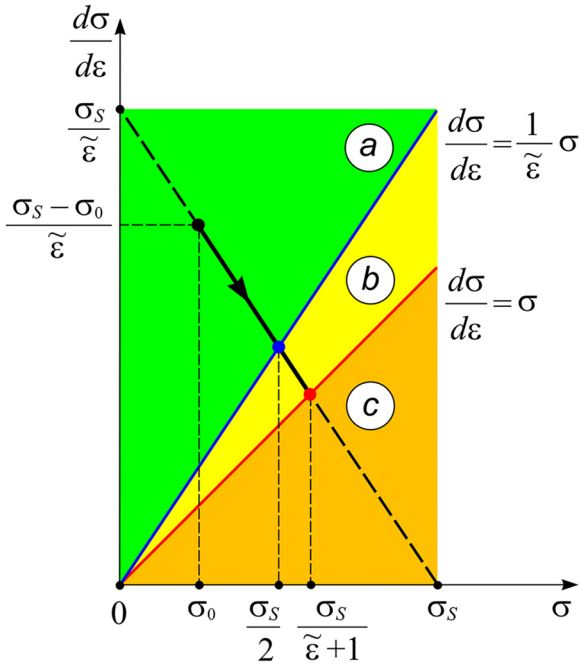

FIG. 5. Diagram of evolution of a material under deformation in the Kocks-Mecking phenomenology in the strain vs hardening coefficient coordinates: (a) stable plastic flow region, (b) plastic flow instability evolution region, and (c) region of global stability loss in the plastic flow.

We can now rewrite the conditions in Eq. (18) in a unified form, and the stresses corresponding to the boundary of the inequalities can be found using Eq. (21):

$$\begin{cases} \frac{1}{\sigma}\frac{d\sigma}{d\varepsilon} > \frac{1}{\tilde{\varepsilon}} \\ \frac{1}{\sigma}\frac{d\sigma}{d\varepsilon} > 1 \end{cases} \Rightarrow \begin{cases} \sigma_1 = \frac{\sigma_S}{2} \\ \sigma_2 = \frac{\sigma_S}{\tilde{\varepsilon}+1} \end{cases}. \tag{22}$$

Using Eq. (20), we depict the evolution of the material during straining with the conditions in Eq. (22) in coordinates $(\sigma; \frac{d\sigma}{d\varepsilon})$ (Fig. 5). The evolution occurs along the black line, with the arrow from the point corresponding to the initial strain hardening. In this case, the Cartesian plane contains three regions: Green (region of stable plastic flow, where both inequalities of the system in Eq. (22) hold; region *a* in Fig. 5), yellow (region of the plastic flow instability evolution, in which only the second inequality of the system in Eq. (22) holds, region *b* in Fig. 5), and orange (global stability loss region of the plastic flow, in which both inequalities of the system in Eq. (22) are invalid; region *c* in Fig. 5). These regions are separated from one another by straight lines $\frac{d\sigma}{d\varepsilon} = \frac{1}{\tilde{\varepsilon}}\sigma$ and $\frac{d\sigma}{d\varepsilon} = \sigma$ (as a rule, $\frac{1}{\tilde{\varepsilon}} = \frac{k_2 M}{2} > 1$ for coarse-grain materials). The evolution of the material begins in the green region of global stability. Further, for $\frac{d\sigma}{d\varepsilon} = \frac{1}{\tilde{\varepsilon}}\sigma$ (blue bullet; in this case, the mechanical stress is $\sigma = \frac{\sigma_S}{2}$), the material is in the yellow region, where instability begins to develop, which terminates with the global loss of stability for $\frac{d\sigma}{d\varepsilon} = \sigma$ (Considère point; red bullet; the mechanical stress in this case is $\sigma = \frac{\sigma_S}{\tilde{\varepsilon}+1}$). In the orange region, a stable plastic flow is impossible. For this reason, the further model evolution in the orange region is depicted by the dashed black line that intersects the mechanical stress axis at hypothetic saturation stress $\sigma = \sigma_S$.

Thus, the approach in the frames of the KM phenomenology reveals two characteristic points corresponding to the conditions in Eq. (22). Using Eq. (21), we can determine the true strain corresponding to these characteristic points:

$$\begin{cases} \frac{1}{\sigma}\frac{d\sigma}{d\varepsilon} = \frac{1}{\tilde{\varepsilon}} \\ \frac{1}{\sigma}\frac{d\sigma}{d\varepsilon} = 1 \end{cases} \Rightarrow \begin{cases} \sigma_1 = \frac{\sigma_S}{2} \\ \sigma_2 = \frac{\sigma_S}{\tilde{\varepsilon}+1} \end{cases} \Rightarrow \begin{cases} \varepsilon_1 = \tilde{\varepsilon}\ln\left[2\left(1-\frac{\sigma_0}{\sigma_S}\right)\right] \\ \varepsilon_2 = \tilde{\varepsilon}\ln\left[\left(1+\frac{1}{\tilde{\varepsilon}}\right)\left(1-\frac{\sigma_0}{\sigma_S}\right)\right] \end{cases}. \tag{23}$$

The experimental loading curves for copper [Fig. 6(a)] and silver [Fig. 6(a)] were approximated by Eq. (21) with the regression coefficient $r^2 = 99.95$. The resulting values of approximation parameters are compiled in Table I and depicted in Fig. 3 by the model curve plotted using these parameters. The values of the true stresses and the true strain corresponding to characteristic points were calculated using the expressions in Eq. (23). The results are compiled in Table I.

Comparing the true stresses in the characteristic interval corresponding to the abrupt change of the Shannon entropy from Table I with the point determined by the condition $\frac{d\sigma}{d\varepsilon} = \frac{1}{\tilde{\varepsilon}}\sigma$ in the KM formulation, it can be noted that the relative error between these two methods does not exceed 10%. We can confidently state that the abrupt change in the Shannon entropy corresponds to the point $(\varepsilon_1; \sigma_1)$ in the KM approach in Eq. (23). At the very beginning of plastic flow, the material deforms heterogeneously—coarse favorably oriented grains yield first. However, the first point of instability which is defined by the condition in Eq. (23) corresponds to true strain of 7–11%, where the deformation is macroscopically uniform. For coarse-grained materials, a homogeneous plastic flow is observed at much lower strains.

Despite its simplicity, the KM model provides an excellent approximation of the strain-hardening curve from the onset of plastic flow to the point of macroscopic instability (Fig. 6). Keeping in mind that the amplitude of AE depends on the dislocation density in a complex manner determined by the interaction of dislocations during strain hardening, the agreement of the AE analysis with the predictions of the KM model indicates that the underlying aspects of dislocation kinetics have been adequately captured. The amplitude of the AE at each moment of time reflects the rate of the elastic energy dissipation during the evolution of the dislocation ensemble. The behavior of the Shannon entropy indicates that this process becomes more complex as the deformation proceeds. We emphasize that the Shannon entropy relates to the dynamics of the energy release, while the configurational entropy characterizes all possible configurations of atoms for a single dislocation. One should bear in mind that AE is a cumulative effect of multiple dislocation reactions involving production, multiplication, and annihilation. In this connection, the increase in the Shannon entropy corresponds to the evolution of the dislocation ensemble to a state where the nonlinear interaction of dislocations dominates.

Since we deal with the deformation of fcc polycrystals, detecting the signs of critical behavior in terms of the dislocation avalanches, as has been done in Refs. [36–40], is challenging. Most studies associating the dislocation avalanche size distribution with the AE amplitude distribution were performed

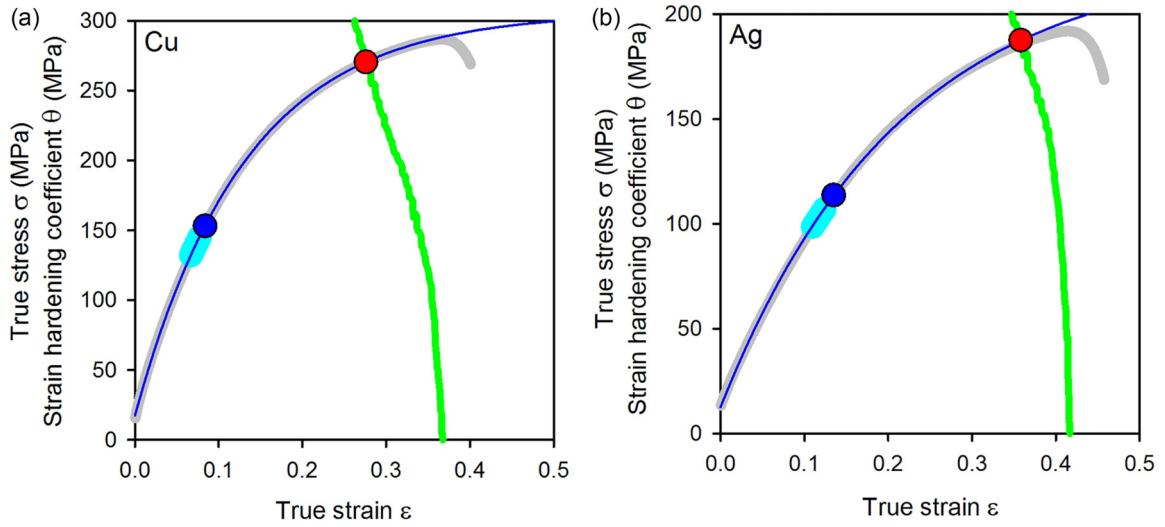

FIG. 6. True stress (gray curves) and strain-hardening coefficient (green curves) as functions of true strain for (a) copper and (b) silver. Blue curves are the results of approximation by Eq. (21) in the Kocks-Mecking phenomenology. Blue and red bullets are the characteristic points obtained from conditions in Eq. (23) and serving as boundaries of the regions in Fig. 5. Turquoise fragments are the characteristic intervals obtained by the recurrence quantification analysis (RQA) method.

on materials with a hexagonal close-packed lattice (Zn, Cd, ice, etc.) exhibiting strong anisotropy and deforming primarily by a single slip mechanism. The exception is copper single crystals investigated among other materials in Ref. [38]. Although the authors found a power-law distribution of AE amplitudes, we note that the number of discrete AE signals distinguishable in the case of copper single crystals [38] is very small, only a few tens. Finally, it should be mentioned that the scale invariance of the dislocation ensemble observed in ice single crystals is violated in polycrystals. Not only the grain boundaries impose a finite-sized effect, but they are also responsible for the triggering effect. In the present case, the number of well-detected discrete AE bursts that can be interpreted as dislocation avalanches is very small. Moreover, the pronounced strain hardening makes it necessary to consider local amplitude distributions in a small time window to reduce the effect of nonstationarity of AE time series. In this case, it is more appropriate to analyze continuous AE signals without detecting individual discrete events, which is implemented in this paper.

The point $(\varepsilon_1;\sigma_1)$ in the KM phenomenology in Eq. (23) has a clear physical meaning. Considering the right-hand side of Eq. (7) as a function of dislocation density, we can easily find that it has a maximum when the condition $\frac{d}{d\rho}(k_1\sqrt{\rho}-k_2\rho)=0$ is met, which leads to the critical dislocation density $\rho* = (\frac{k_1}{2k_2})^2$. Using the Taylor formula in Eq. (11), we can find stress $\sigma* = \beta\sqrt{\rho*} = \frac{\beta k_1}{2k_2} = \frac{\sigma_S}{2} = \sigma_1$ corresponding to this dislocation density. Therefore, the characteristic point determined by the condition $\frac{d\sigma}{d\varepsilon} = \frac{1}{\tilde{\varepsilon}}\sigma$ in the KM phenomenology corresponds to the maximal growth rate of the dislocation density.

On the other hand, the second characteristic point $(\varepsilon_2;\sigma_2)$ determined by the condition $\frac{d\sigma}{d\varepsilon} = \sigma$ is the classical Considère point describing the global stability loss with the formation of a neck followed by sample fracture. This point indicates the

TABLE I. The characteristic points determined from the analysis of AE signals by the RQA method and proceeding from the Kocks-Mecking phenomenology. Red and blue colors correspond to the red and blue bullets in Fig. 6.

Determined parameters		Metal	
		Cu	Ag
Characteristic intervals of experimental parameters determined by the RQA method and corresponding to the change in the information entropy trend	t, s	64.2–74.7	104.9–118.0
	ε	0.07–0.08	0.11–0.12
	σ, MPa	131–145	99–107
Values of parameters of approximation of experimental data by Eq. (21) in the Kocks-Mecking phenomenology	σ_0, MPa	17.50	12.60
	σ_S, MPa	306.14	227.36
	$1/\tilde{\varepsilon}$	7.59	4.70
Values of true strain and true stress corresponding to the characteristic points in the Kocks-Mecking phenomenology in accordance with the expressions in Eq. (23)	ε_1	0.08	0.13
	σ_1, MPa	153	114
	ε_2	0.28	0.36
	σ_2, MPa	270	187

complete degradation of the material after the attainment of stress σ_2. The functional relation between the parameters of the first and second characteristic points can easily be obtained from the conditions in Eq. (23):

$$\varepsilon_2 = \varepsilon_1 + \tilde{\varepsilon}\ln\left(\frac{\tilde{\varepsilon}+1}{2\tilde{\varepsilon}}\right)$$
$$\sigma_2 = \frac{2\sigma_1}{\tilde{\varepsilon}+1}. \tag{24}$$

Therefore, if the RQA of the AE time series shows the first sharp increase in the Shannon information entropy from the initial trend, the mechanical stress corresponding to this point is connected by the clear functional relation in Eq. (24) with the mechanical stress corresponding to the global stability loss of the plastic flow. The only control parameter of the above functional dependences is a parameter $\tilde{\varepsilon} = \frac{2}{k_2 M}$; however, the dislocation dynamic recovery coefficient k_2 for coarse-grain materials typically ranges between 1 and 10.

In conclusion, because of the RQA of AE time series, a characteristic interval of the rapid increase of the Shannon information entropy was found. Physical interpretation of the found characteristic interval at the beginning of plastic flow stability loss was proposed based on a fluctuation analysis of dislocation ensemble behavior. With the appropriate calibration, the proposed RQA approach offers a fundamental basis for developing diagnostic systems capable of forecasting the critical state of a material and indicating the safe intervals for the operation of different mechanisms. To this end, the effects of loading conditions and metallurgical factors need to be incorporated explicitly in the upcoming research.

ACKNOWLEDGMENTS

E.A.A. is grateful to the Russian Science Foundation for support (Project No. 22–72–00117). The authors are grateful to Prof. A. Vinogradov for his encouragement and numerous insightful discussions.

E.A.A.: Conceptualization, methodology, software, writing—original draft, investigation, writing—review and editing, and visualization. I.S.Y.: Conceptualization, investigation, and writing—original draft.

The authors declare that they have no known competing financial interests or personal relationships that could have appeared to influence the work reported in this paper.

[1] J. P. Eckmann, S. O. Kamphorst, and D. Ruelle, Europhys. Lett. **4**, 973 (1987).
[2] M. T. Rosenstein, J. J. Collins, and C. De Luca, Physica D **65**, 117 (1993).
[3] L. R. Gorjão, G. Hassan, J. Kurths, and D. Witthaut, Comput. Phys. Commun. **273**, 108254 (2022).
[4] P. Grassberger and I. Procaccia, Phys. Rev. Lett. **50**, 346 (1983).
[5] G. Zimatore, G. Garilli, M. Poscolieri, C. Rafanelli, F. T. Gizzi, and M. Lazzari, Chaos **27**, 043101 (2017).
[6] N. V. Zolotova and D. I. Ponyavin, Astron. Astrophys. **449**, L1 (2006).
[7] R. Pánis, M. Kološ, and Z. Stuchlík, Eur. Phys. J. C **79**, 479 (2019).
[8] G. Orlando, G. Zimatore, and A. Giuliani, in *Nonlinearities in Economics* (Springer Nature, Cham, 2021), pp. 141–150.
[9] G. Zimatore, M. Cavagnaro, P. H. Skarzynski, and S. Hatzopoulos, Clin. Interv. Aging **15**, 927 (2020).
[10] Z.-B. Wu, Phys. Lett. A **332**, 250 (2004).
[11] A. Vinogradov, I. S. Yasnikov, and Y. Estrin, J. Appl. Phys. **115**, 233506 (2014).
[12] I. S. Yasnikov and A. Yu. Vinogradov, J. Exp. Theor. Phys. **132**, 394 (2021).
[13] Z. Zhang, Z. Zhao, P. Bai, X. Li, B. Liu, and X. Wu J.Tan, J. Alloys Compd. **878**, 160334 (2021).
[14] L. Hilarov, Phys. Solid State **57**, 2271 (2015).
[15] T. Matcharashvili, T. Chelidze, N. Zhukova, and E. Mepharidze, Tribol. Int. **44**, 811 (2011).
[16] E. N. Lorenz, J. Atmospheric Sci. **20**, 130 (1963).
[17] H. Kantz and T. Schreiber, *Nonlinear Time Series Analysis*, 2nd ed. (Cambridge University Press, Cambridge, 2004).
[18] F. Takens, *Dynamical Systems and Turbulence*, edited by D. Rand and L. S. Young, Lecture Notes in Mathematics, Vol. 898 (Springer, Berlin, 1981).
[19] A. M. Fraser and H. L. Swinney, Phys. Rev. A **33**, 1134 (1986).
[20] L. Cao, Physica D **110**, 43 (1997).
[21] N. Marwan, N. Wessel, U. Meyerfeldt, A. Schirdewan, and J. Kurths, Phys. Rev. E **66**, 026702 (2002).
[22] C. L. Webber, Jr. and J. P. Zbilut, J. Appl. Physiol. **76**, 965 (1994).
[23] L. L. Trulla, A. Giuliani, J. P. Zbilut, and C. L. Webber, Jr., Phys. Lett. A **223**, 255 (1996).
[24] A. V. Danyuk, D. L. Merson, I. S. Yasnikov, E. A. Agletdinov, M. A. Afanasiev, and A. Vinogradov, Lett. Mater. **7**, 437 (2014).
[25] A. Vinogradov, A. V. Danyuk, D. L. Merson, and I. S. Yasnikov, Scr. Mater. **151**, 53 (2018).
[26] A. Vinogradov, I. S. Yasnikov, and D. L. Merson, Scr. Mater. **170**, 172 (2019).
[27] A. Considère, Ann. Ponts Chaussées. **9**, 574 (1885).
[28] F. Kocks and H. Mecking, Prog. Mater Sci. **48**, 171 (2003).
[29] A. Vinogradov, I. S. Yasnikov, and Y. Estrin, Phys. Rev. Lett. **108**, 205504 (2012).
[30] M. Stricker, M. Sudmanns, K. Schulz, T. Hochrainer, and D. Weygand, J. Mech. Phys. Solids **119**, 319 (2018).
[31] M. Sudmanns, M. Stricker, D. Weygand, T. Hochrainer, and K. Schulz, J. Mech. Phys. Solids **132**, 103695 (2019).
[32] C. Keller and E. Hug, Int. J. Plast. **98**, 106 (2017).
[33] Y. Estrin and H. Mecking, Acta Metall. **32**, 57 (1984).

[34] I. S. Yasnikov, A. Vinogradov, and Y. Estrin, Scr. Mater. **76**, 37 (2014).
[35] A. Sendrowicz, A. O. Myhre, I. S. Yasnikov, and A. Vinogradov, Acta Mater. **237**, 118190 (2022).
[36] M. C. Miguel, A. Vespignani, S. Zapperi, J. Weiss, and J. R. Grasso, Nature (London) **410**, 667 (2001).
[37] J. Weiss and D. Marsan, Science **299**, 89 (2003).
[38] J. Weiss, T. Richeton, F. Louchet, F. Chmelik, P. Dobron, D. Entemeyer, M. Lebyodkin, T. Lebedkina, C. Fressengeas, and R. J. McDonald, Phys. Rev. B **76**, 224110 (2007).
[39] D. M. Dimiduk, C. Woodward, R. LeSar, and M. D. Uchic, Science **312**, 1188 (2006).
[40] P. D. Ispánovity, D. Ugi, G. Péterffy, M. Knapek, S. Kalácska, D. Tüzes, Z. Dankházi, K. Máthis, F. Chmelík, and I. Groma, Nat. Commun. **13**, 1975 (2022).